RSC Advances

PAPER

View Article Online
View Journal | View Issue

Cite this: *RSC Adv.*, 2016, **6**, 56698

Evolution of the reaction mechanism during the MTH induction period over the 2-dimensional FER zeolite†

Liang Qi,[ab] Jinzhe Li,[a] Lei Xu*[a] and Zhongmin Liu*[a]

Received 10th April 2016
Accepted 26th May 2016

DOI: 10.1039/c6ra09237c

www.rsc.org/advances

The methanol conversion reaction mechanism over HZSM-35, an ferrierite (FER)-type zeolite with 2-D channel intersections, was investigated during the induction period. The MTH induction period could be obviously shortened by co-feeding toluene or precoking the catalyst and the formation of tetramethylcyclopentenyl cation (tetraMCP+) during the induction period was also confirmed through ^{13}C magic angle spinning (MAS) NMR and GC-MS experiments, suggesting the active role of aromatics. Moreover, the dual-cycle mechanism was evidently found to evolve as the induction reaction progressed. In the early stage, both the aromatic- and olefin-based routes work efficiently and pentamethylbenzene (pentaMB) was identified as the main aromatic hydrocarbon pool (HCP) species. While in the latter stage of the induction period, the olefin-based route turned out to be more dominant and pentaMB as well as hexamethylbenzene (hexaMB) became the main aromatic HCP species. Despite the limited space of the channel intersections, the reactivity of aromatics with larger molecular sizes like 1-ethyl-2,3,4,5,6-pentamethylbenzene (1-E-pentaMB) and hexaMB were much higher than lower methylbenzenes which indicates that the aromatic-based cycle can also proceed on the external acid sites of the HZSM-35 catalyst.

1 Introduction

In recent years, the increasing global energy demand together with the decreasing supplies of traditional petroleum resources make it increasingly hard to supply the world with fuels and chemicals. As a result, the development of nontraditional carbon-based processes to produce fuels or light olefins is essential. The methanol-to-hydrocarbon (MTH) processes including methanol-to-gasoline (MTG), methanol-to-olefins (MTO), methanol-to-propene (MTP) and methanol-to-aromatics (MTA) have become promising since the methanol feedstock can be produced *via* a syngas intermediate from a variety of gasifiable carbon-based feedstocks, such as natural gas, coal, and biomass.[1–5]

MTH reaction is a well-known typical autocatalytic process, during which the induction period, the steady-state period and the deactivation period are involved.[1,6] To design and synthesize efficient catalyst with high selectivity of aim product, great efforts have been devoted to understand the reaction mechanism. Up to date, due to the complexity of this system, more than 20 reaction mechanisms have been proposed during the last few decades,[2,6–10] among which the hydrocarbon pool (HCP) mechanism has gained general acceptance based on experimental observations as well as theoretical calculations.[3,11–14] As suggested, methanol is added and olefins can be eliminated in a closed catalytic cycle with HCP species as a catalytic scaffold.[3,13–17] Accordingly, the combination of HCP species and zeolite framework should be the true working catalyst as a supramolecular complex.[3,13–17]

Since the proposal of HCP mechanism, investigation of the HCP species has ignited great enthusiasm.[5,18–22] Generally speaking, aromatic species (like methylbenzenes and polymethylnaphthalenes) were initially regarded as main HCP species over zeolite catalyst.[13–17] With the aid of solid-state NMR spectroscopy (ssNMR), many carbenium ions have been successfully and directly captured and investigated under real methanol conversion conditions. According to previous reports, the methylcyclopentadienyl cations, indanyl, and 1,1,2,4,6-pentamethylbenzenium have been identified over HZSM-5 zeolite while heptamethylcyclopentenyl, heptamethylbenzenium cation and pentamethylcyclopentenyl cation have been identified within CHA-type catalysts.[17,23–29] Investigation of the carbenium ions helps understand the participation of aromatic speices in the MTH reaction more deeply and clearly and the aromatic compounds are considered to participate in the MTH

[a]*National Engineering Laboratory for Methanol to Olefins, Dalian National Laboratory for Clean Energy, iChEM (Collaborative Innovation Center of Chemistry for Energy Materials), Dalian Institute of Chemical Physics, Chinese Academy of Sciences, Dalian 116023, People's Republic of China. E-mail: liuzm@dicp.ac.cn; leixu@dicp.ac.cn; Fax: +86 411 84379998; Tel: +86 411 84379998*

[b]*University of Chinese Academy of Sciences, Beijing 100049, People's Republic of China*

† Electronic supplementary information (ESI) available. See DOI: 10.1039/c6ra09237c

reaction in two reaction routes, namely the side-chain methylation route and the paring route.[30–32] Specifically, the side-chain mechanism proceeds through the methylation of methylbenzenes or carbenium cations following with elimination of side-chain groups to produce olefins. While the paring route involves the contraction of six-membered ring cations and the expansion of five-membered ring cations which splits off alkenes.[30–32]

Thus far, the HCP mechanism has been proved quite convincing and can be accountable for different MTH reaction stages. However, considering the complex composition of coke species and the underlying various reaction routes, the HCP mechanism is still extremely intricated. In addition, the detailed HCP mechanism varies considerably with the zeolite topology and it was concluded that the molecular size and reactivity of confined species was obviously influenced by the size of cavity and channel intersections.[39] The silicoaluminophosphate catalyst HSAPO-34 is a well-known chabazite (CHA) structure that features cages (6.7 × 10 Å) interconnected through windows which are eight atom rings, *ca.* 0.38 nm. While HZSM-5 is a three dimensional channel zeolite based on 10-atom rings *versus* the in HSAPO-34, and it contains two types of interconnecting channels: straight channels (5.6 × 5.3 Å) and sinusoidal channels (5.5 × 5.1 Å). It is now popularly known that, over cage-type zeolite like HSAPO-34, ethene and propene are the main volatile products and the methanol conversion reaction mainly goes through the aromatic-based HCP mechanism and polymethylbenzenes like hexaMB are the most active aromatic compound.[3] While over zeolite without cages but channel intersections like HZSM-5 catalyst certain amount of higher olefin and alkane products as well as aromatics can be found and Olsbye *et al.* found that aromatic species with smaller size were more active.[18] Moreover, besides carbenium and polymethylbenzenes (polyMBs), olefins may also act as another kind of active HCP species over HZSM-5.[11,12] This leads to the proposal and establishment of the ''dual-cycle'' mechanism: in one cycle products are generated by repeated olefins methylation and cracking step, while in the aromatics cycle light olefins are tend to be formed by continuously methylated and dealkylated steps.[11,12] Both of the two cycles work efficiently during the methanol conversion reaction over HZSM-5 catalyst. Thereafter, it was further proved that the dual-cycle mechanism also changes significantly over catalysts with different type of channel intersections. For HZSM-22 catalyst, a zeolite material with 1-D channel, the aromatic-based cycle is relatively less effective compared with HZSM-5 catalyst and the methanol conversion reaction mainly follows the olefin-based cycle.[33–35] Besides, it was found that, over both HZSM-22 and HZSM-23 zeolites, the external acid sites and pore mouth catalysis also play a key role in the production of olefins through the HCP mechanism.[36]

Conclusively, the zeolite topology can imposes a significant influence on the detailed reaction mechanism, which may include the molecular size and reactivity of confined species, the inter-relation of dual-cycle mechanism. HZSM-35 is a typical FER-type zeolite with 2-D channel intersections (the structure features 10-ring channels running in one direction and 8-ring channels in a second direction), the space of which is larger than that of the 1-D HZSM-22 but smaller than that of the 3-D HZSM-5.[3] The skeletal structure of HZSM-35 is shown in Fig. S3.† As reported earlier, butenes and pentenes are the main olefin products over the FER catalyst.[3] Moreover, due to the insufficient room in the FER channels, the cyclization and intramolecular hydride transfer reactions may be hindered.[3] Up to now, the recognition of HCP mechanism over the HZSM-35 catalyst is still not clear but is of great significance due to its unique topology. In this research, the reaction mechanism during the MTH induction period over HZSM-35 catalyst was investigated. The active role of aromatics was proved and it was interestingly found that higher methylbenzenes can also act as active centers over the external acid sites. Moreover, the evolution of the dual-cycle mechanism during the induction period was also investigated.

2 Experimental section

2.1 Preparation of the catalysts

ZSM-35 samples (Si/Al = 15) were prepared according to a former report.[37] The calcined samples were ion exchanged with a NH_4NO_3 aqueous solution (1 M) for 2 h at 80 °C followed by washing with deionized water for 1 h at 70 °C for twice. Then the samples were dried at 110 °C for 12 h and calcined in air at 550 °C for 10 h to obtain the protonated HZSM-35 samples.

2.2 Characterization of the catalysts

The powder XRD pattern was recorded on a PANalytical X'Pert PRO X-ray diffractometer with Cu-Kα radiation ($\lambda = 1.54059$ Å), operating at 40 kV and 40 mA. The crystal morphology was observed by field emission scanning electron microscopy (Hitachi, SU8020).

2.3 Extraction and GC-MS analysis of the confined organics

The coked catalyst (50 mg) was first dissolved in 1.0 mL of 15% HF in a Teflon vial. The obtained organic mixture was then extracted with 0.5 mL CH_2Cl_2. The organic phase was analyzed using an Agilent 7890A/5975C GC/MSD.

2.4 Catalytic tests

The zeolite samples were pressed and sieved into a fraction of 40–60 mesh and 1 g of it was loaded in a fixed-bed stainless steel tubular reactor (9 mm i.d.) at atmospheric pressure. Then quartz sand was loaded to the upper and lower part of the reactor to get a plug flow of the mixed feed. Prior to the introduction of reactants, the catalyst was activated *in situ* at 550 °C under a flow of air (20 mL min^{-1}) for 1 h and then cooled to reaction temperature.

Methanol was pumped into the reactor with a space velocity of 4 h^{-1}. For the toluene co-feeding experiment, toluene was directly mixed with methanol. In order to avoid the product solidification, the outlet line was twined with the heat tape to keep the temperature at 220 °C. The effluent was analyzed by on-line gas chromatography (Angilent GC7890A) equipped with a FID detector and a PoraPLOT Q-HT capillary column.

2.5 ^{13}C MAS NMR measurement of methanol conversion

Methanol conversion over HZSM-35 was measured by ^{13}C solid-state NMR employing ^{13}C-methanol as the reactant. Under the same conditions of ^{12}C-methanol conversion, ^{13}C-methanol was fed into the reactor for a predetermined time. Then the reactor was removed from the feeding line, and the catalyst was cooled down very quickly by putting them into the vessel containing liquid nitrogen. Finally, the cooled catalyst was transferred to an NMR rotor in a glove box without exposure to ambient air.

2.6 ^{12}C/^{13}C-methanol switch experiment

In the ^{12}C/^{13}C-methanol switch experiments, after 5 min and 20 min of ^{12}C-methanol conversion reaction respectively, the feeding line was switched to ^{13}C-methanol for further 1.5 min. The isotopic distribution of the effluent products and the species confined in the catalyst were determined by GC-MS (Agilent 7890/5975C).

3 Results and discussion

3.1 General phenomenon of the MTH induction reaction

According to the characterization results, Powder XRD confirmed that the prepared sample consisted of a pure and well crystalline FER phase (Fig. S1†). SEM images showed that the samples consist of uniform flake-shape crystals which is the typical morphology of FER-type zeolites reported previously[37] (Fig. S2†).

The methanol conversion reaction was first performed at a higher temperature range (320–450 °C). It's clearly seen that the catalyst is very easy to be deactivated. Even when the temperature was increased to 450 °C (Fig. 1(b)), the catalyst lifetime can last only 60 min which may be attributed to the poor diffusivity of the catalyst. To clearly observe the induction period, methanol conversion reaction was further conducted at a lower temperature range of 270 °C to 300 °C over HZSM-35 zeolite and the corresponding change of methanol conversion with time on stream (TOS) was shown in Fig. 1(a). At 300 °C, the methanol conversion at 2 min was negligibly low and then increased rapidly to *ca.* 10% at 22 min, which means an obvious induction period exists in the MTH reaction. At a lower temperature of 280 °C, the methanol conversion at 22 min was only *ca.* 0.4% and then increased gradually to 3% at 100 min. This suggests that the MTH reaction behaviors and induction periods were quite sensitive to the temperature and lowering down reaction temperature prolongs the induction period. The induction period could be as long as several hours when the temperature is lowered to 270 °C. Almost no methanol conversion was observed (<0.3%) before 100 min. After 100 min, an obvious auto-catalytic MTH reaction was observed even the methanol conversion was still very low (<1%) before 200 min. As was reported earlier, during the induction period, sufficient HCP species formed and accumulated to trigger obvious MTH reaction.[6] The long induction period implies that the formation of HCP species could be quite difficult at low reaction temperature over HZSM-35 catalyst. In addition, the catalyst deactivated rapidly after the methanol conversion reaches to a maximum value.

Detailed product distribution with TOS at 270 °C was shown in Fig. 2(b). CH_4 and C_2H_4 were the initially detectable product, while C_3H_6 and C_5 were not detectable until 42 min. The selectivity of all the effluent products kept unchanged during the autocatalysis reaction stage. This corresponds with our previous report very well.[6]

3.2 Clarifying the role of aromatics in the MTH induction reaction

It was recently reported that a critical amount of HCP species should be generated and accumulated to trigger the MTH reaction during the induction period over HZSM-5 catalyst.[6] A long induction period was observed in Fig. 2(a), suggesting the low formation rate of HCP species at low reaction temperature over HZSM-35 catalyst. It has been proved that methylbenzenes as well as methylnaphthalenes can act as the major active HCP species over HZSM-5 and HSAPO-34 catalysts.[28,38–40] Moreover, we have found that addition of trace amount of toluene could obviously shorten the MTH induction period over HZSM-5 catalyst.[6] The diameters of the 10-ring channels run in HZSM-5 are approximately 10% greater than that of HZSM-35.[3] To introduce aromatics into the catalyst channels efficiently, aromatic with small size like toluene was selected in the present co-feeding reaction (the introduced amount is 100 ppm) to investigate the role of aromatics during the MTH induction reaction over HZSM-35 catalyst.

As is shown in Fig. 3, the methanol conversion reaction was promoted after co-feeding certain amount of aromatics. With the addition of toluene, the methanol conversion increased

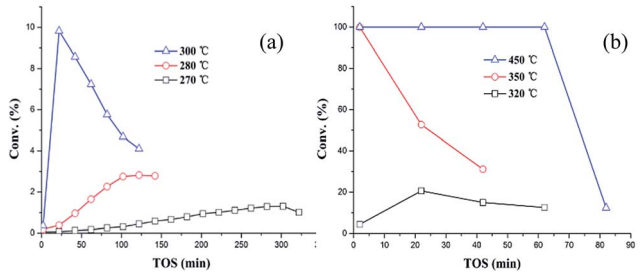

Fig. 1 Conversion of methanol on HZSM-35 zeolite as a function of reaction time at low (a) and high (b) reaction temperature ranges.

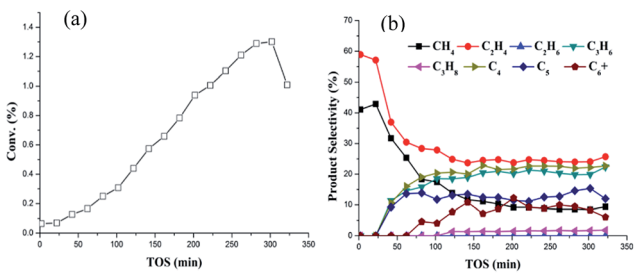

Fig. 2 Methanol conversion (a) and effluent distribution (b) as a function of time on stream (TOS) during the MTH reaction at 270 °C.

more rapidly since the very beginning of the reaction while the increasing rate slowed down after *ca.* 150 min. In addition, for the co-feeding system, the maximum methanol conversion was 1.1%, lower than that obtained during the pure methanol conversion (1.3%). While for the toluene co-feeding experiment over HZSM-5 catalyst, the induction period was more evidently shortened and the maximum methanol conversion was also greatly enhanced.[6] Consequently, the promoting effect of aromatics seemed less effective over HZSM-35 compared with that over HZSM-5 catalyst.[6] There may exist two reasons for this phenomenon. On one hand, it may be due to the poorer diffusivity of ZSM-35 zeolite with 2-D channels (10-ring × 8-ring) compared with ZSM-5 material with 3-D channels (10-ring × 10-ring × 10-ring). As a result, the introduced toluene can't effectively diffuse into the HZSM-35 catalyst through the 10-ring channels functioning as active HCP species. Moreover, the limited diffusivity should also be accountable for the advanced deactivation behavior. On the other hand, the weak promoting effect of the introduced aromatics may be caused by its intrinsic low autocatalytic effect over the FER zeolite. Both these two factors seems reasonable and the activity of aromatics during the MTH reaction on HZSM-35 catalyst is still unclear without further investigation.

To further clarify the effect of aromatic species on the MTH reaction over HZSM-35 catalyst, a pre-coked catalyst was prepared for the test. The pre-coked sample was prepared as follows: the methanol conversion reaction was performed at 300 °C for 5 min, after that the catalyst was purged with 20 mL min^{-1} He for 20 min. Then the reaction temperature was lowered down and the MTH reaction over the pre-coked catalyst was carried out at 270 °C, the experiment result was shown in Fig. 4. The promoting effect of the pre-formed retained species is clearly presented, the pre-coked samples had a much higher initial activity compared with the fresh one. No induction period could be observed and it deactivated rapidly since the very beginning of the MTH reaction. This result helps consolidate that aromatic species can act as active reaction centers over HZSM-35 catalyst during the MTH induction reaction despite the restricted space of the channel intersections.

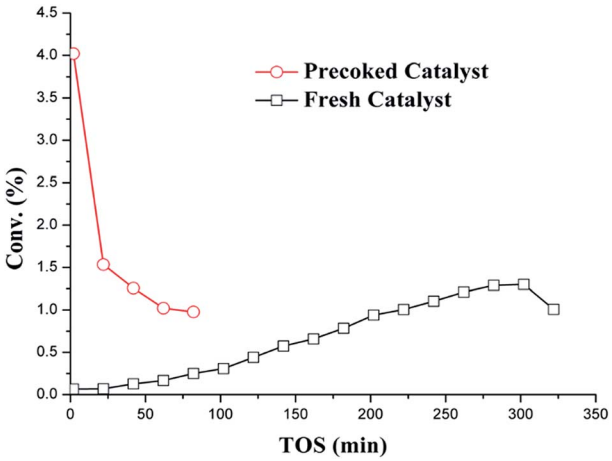

Fig. 4 Methanol conversion as a function of time on stream during the MTH reaction over fresh catalyst and pre-coked catalyst at 270 °C.

3.3 Analysis of retained species during the MTH induction reaction

3.3.1 GC-MS analysis of retained species. It's well acknowledged that the molecular size and reactivity of the confined aromatic species are closely related with the size of cavity or channel intersections of the catalysts.[39] Moreover, it's recently reported that pentaMB is the major aromatic active species on HZSM-5 catalyst while hexaMB and methylnaphthalenes are proved to be the dominant active species over HSAPO-34 catalysts.[41,42] Despite the recognition that aromatics can promote the methanol conversion reaction on HZSM-35 catalyst, the composition of the coke species and the relative reactivity of them is still unknown. Fig. 5(a) shows the GC-MS total ion chromatogram of the organics deposited inside the zeolite after 5 min of methanol reaction at 300 °C. It can be seen that polyMBs were dominant among the retained organics. PentaMB is most abundant, followed by tetramethylbenzenes (tetraMBs), hexaMB, trimethylbenzenes (triMBs), and *p*/*m*-xylene. Besides, a small amount of hydrocarbons with larger molecular mass than hexaMB like 1-E-pentaMB and methylnaphthalenes were also detected. Previous studies presented the similar results for the organics formed inside HZSM-5

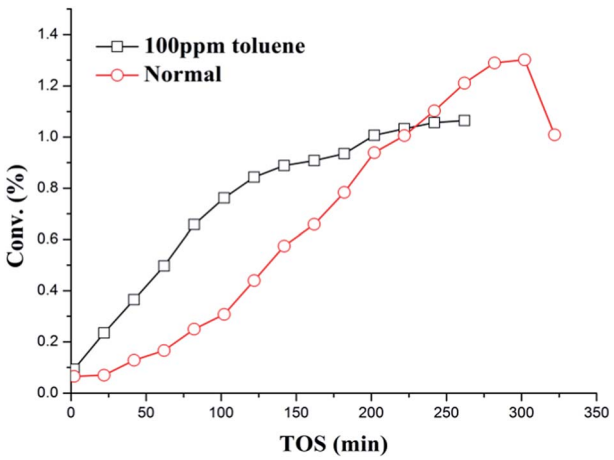

Fig. 3 Effect of co-feeding 100 ppm toluene on methanol conversion during the MTH reaction over HZSM-35 catalyst at 270 °C.

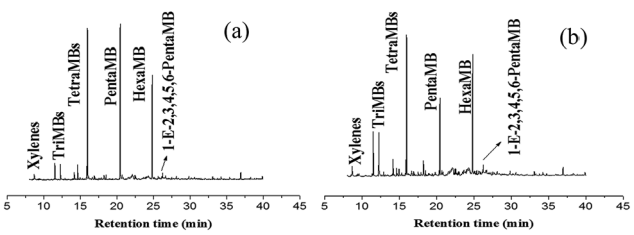

Fig. 5 GC-MS results of retained species in catalyst under different reaction conditions: (a) $T = 300$ °C, TOS = 5 min; (b) $T = 300$ °C, TOS = 20 min.

catalyst under MTH conditions. When the reaction time was further prolonged to 20 min, the concentration of lower methylbenzenes was increased and the dominant species of the retained species turned to tetraMBs (Fig. 5(b)).

3.3.2 Observation of carbocations. Carbenium ions are important reaction intermediates and the existence of them provides us an evidence of the aromatic-based cycle during the MTH reaction. Fig. 6(b) shows the ^{13}C MAS NMR spectra of the retained organic species after 20 min of ^{13}C methanol reaction at 300 °C. The strong signals at 50.5 and 60.5 ppm represented the physisorbed methanol and dimethyl ether in the catalyst.[43–45] The ^{13}C signals at 15.5, 24.8, 127 and 136 ppm indicated the presence of alkylated aromatics such as methylbenzenes according to a previous report.[41] The strong signals between 10 and 50 ppm represented the carbon atoms from alkyl groups while the signals at 128 ppm was assigned to carbon atoms in the benzene ring of the retained aromatics.[41] Besides the stable organic species mentioned above, the characteristic signals at 249, 154 and 152 ppm indicating the formation of the important five-membered ring cations, polymethylcyclopentenyl cations (PMCPs),[29,46] which were also observed over HZSM-35. The PMCPs have been proved to be a very important reaction intermediate during MTH conversion.[29] At the same time, another kind of important carbenium ion, benzenium ion, which has been reported previously,[46] was not detected in the present work, possibly due to their high reactivity and extreme instability during the reaction.

The retained methylcyclopentadiene compounds in the HZSM-35 catalyst were also found in the GC-MS chromatogram (Fig. 6(a)). According to the library of NIST11, the peaks at retention times of 12.9 min were assigned to tetraMCPs. More importantly, these deprotonated forms of methylcyclopentenyl cations confirmed the formation of PMCPs detected in the NMR measurement. As an important reaction intermediate, the successful capture of tetraMCP+ helps further prove the active participation of aromatics in the MTH induction reaction.

3.4 Evolution of reaction mechanism during the MTH induction reaction

3.4.1 Reaction mechanism in the early stage of induction period. $^{12}C/^{13}C$-methanol switch experiments were conducted to distinguish the reactivity of trapped aromatic species in the catalyst during methanol conversion. The total ^{13}C contents of the retained organic species on the catalyst and effluent alkenes after the switch experiments are shown in Fig. 7. Among the retained organics, pentaMB exhibited highest ^{13}C content than other methylbenzenes retained in HZSM-35, implying its highest reactivity as important intermediates during the induction period of the reaction. Moreover, it should be mentioned that pentaMB was the major aromatic species during the initial stage of MTH induction reaction (Fig. 5(a)). Considering the highest reactivity of pentaMB, it can be regarded as the main active HCP species under current condition. These results are partly in accordance with what Feng Deng *etc.* recently found on HZSM-5 catalyst: pentaMB were more reactive than other methylbenzenes.[42]

According to the previous research, hexaMB has been proved to an inactive aromatic species over HZSM-5 catalyst.[12] However, it was obviously seen that the reactivity of hexaMB was higher than triMBs and the ^{13}C content of it was almost three times of that of xylenes. More interestingly, it was found that the reactivity of 1-E-pentaMB, aromatic with a larger molecular size, was even higher than hexaMB. As is mentioned above, there exist a confinement effect of the zeolite topology on the molecular size and reactivity of the retained aromatic species. This result seems contradictory at first sight. It has been reported that the external acid sites and pore mouth catalysis also play a key role

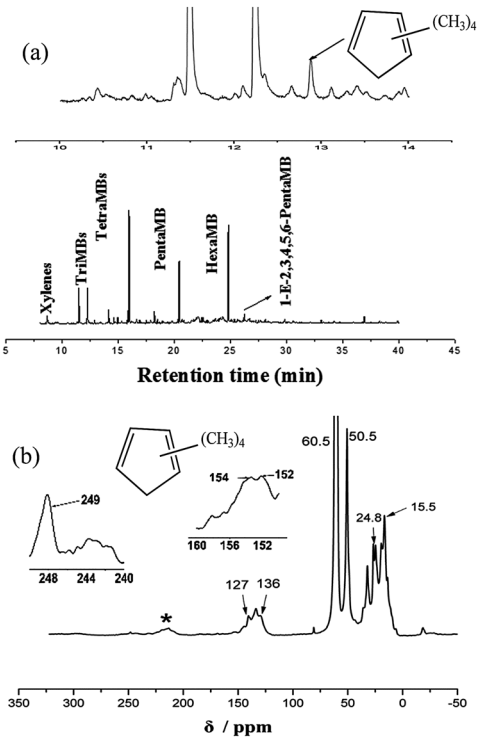

Fig. 6 GC-MS analysis of retained material in catalyst after continuous-flow ^{13}C-methanol reaction for 20 min at 300 °C (a) and ^{13}C CP MAS NMR spectra of HZSM-5 with retained organics after continuous-flow ^{13}C-methanol reaction for 20 min at 300 °C (b). The asterisk denotes spinning side bands.

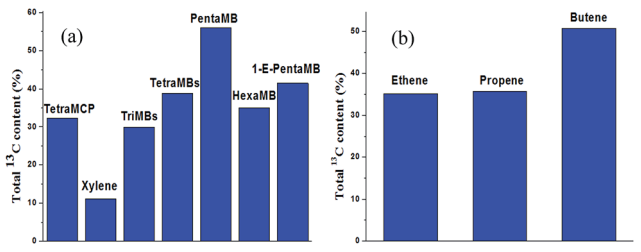

Fig. 7 The total ^{13}C content of the retained organic materials (a) and the effluent products (b) after the $^{12}C/^{13}C$ switch experiment over HZSM-35 at 300 °C with 5 min ^{12}C-methanol feeding during the MTH reaction, followed by 1.5 min of ^{13}C-methanol feeding.

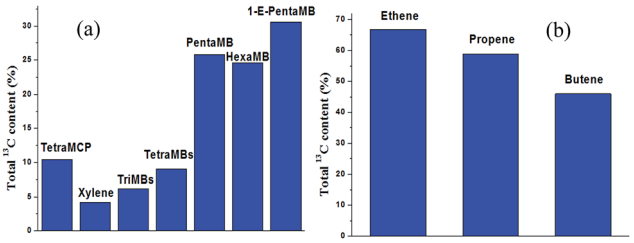

Fig. 8 The total ^{13}C content of the retained organic materials (a) and the effluent products (b) after the ^{12}C/^{13}C switch experiment over HZSM-35 at 300 °C with 20 min ^{12}C-methanol feeding during the MTH reaction, followed by 1.5 min of ^{13}C-methanol feeding.

in the production of olefins on ZSM-22 and ZSM-23 zeolites through the hydrocarbon pool mechanism.[36] Moreover, the flake-shape of ZSM-35 crystals can be easily stacked together and the aromatics may function as active HCP species in the inter-crystalline pores. Thereafter, it can be supposed that aromatic species with larger molecular size can also act as active centers over the external acid sites.

The ^{13}C content of ethene and propene were close to that of tetraMB and tetraMCP, implying the participation of these retained active HCP species in the generation of ethene during the induction period.[11,12] The ^{13}C content of higher alkene products like butenes was higher than that of ethene and propene which suggested the generation of higher alkene possibly followed the olefin methylation and cracking route. The result of ^{12}C/^{13}C-methanol switch experiments at TOS = 5 min indicated that both the aromatic- and olefin-based cycle work efficiently in the earlier stage of the induction period.

3.4.2 Reaction mechanism in the latter stage of induction period. When the reaction time was prolonged to 20 min, the methanol conversion reached a maximum value and was followed by a rapid deactivation, which may be ascribed to the block of zeolite channels. The ^{13}C content of retained organics in HZSM-35, such as tetraMCP, xylene, triMBs and tetraMBs, became very little involved in the alkene formation as shown in Fig. 8(a). While the ^{13}C content of the effluent hydrocarbons was much higher than that of the retained organic materials, suggesting that the olefin-based cycle became the most dominant reaction route in the latter stage of the MTH induction period.[11,12,33] It should be mentioned that the ^{13}C content of the effluent olefin products decreased in the order of ethene > propene > butene. This is probably caused by the deactivation of the HZSM-35 catalyst. The catalyst channels were partly blocked and the successive methanol conversion reaction was hindered which could further suppress the methylation of olefin effluent. However, the higher olefins can also be cracked to form lighter ones and as a result, the content of ^{13}C atoms in ethene was higher than that of higher alkene products.

Besides the reduced reactivity of all the confined organics, the activity order of the retained species also changed obviously. The reactivity of the retained methylbenzens decreased in the order of 1-E-pentaMB > pentaMB > hexaMB > tetraMBs > triMBs > xylenes, which is almost in accordance with the decreasing order of their molecular size. The ^{13}C content of 1-E-pentaMB, pentaMB and hexaMB were much higher than that of the others and 1-E-pentaMB with the biggest molecular size was observed as the most reactive retained species. Moreover, according to the GC-MS analysis (Fig. 5(b)), pentaMB and hexaMB were the major aromatic species under current condition. Considering the high reactivity of pentaMB and hexaMB, they turned to be the main active HCP species during the latter stage of MTH induction period. At this point, the catalyst began to deactivate and aromatic molecular with the larger size should be less active due to the steric effect in the ZSM-35 channels. However, as proposed above, the aromatic-based cycle may also proceed on the external acid site of HZSM-35 catalyst. As a result, the observed higher reactivity of 1-E-pentaMB, and hexaMB further provide us a direct evidence for the supposal.

4 Conclusions

The MTH induction reaction mechanism over HZSM-35 was investigated in detail. Aromatic compounds were proved to be active HCP species and introduction of them could shorten the MTH induction period. Moreover, the dual-cycle mechanism was found to evolve evidently as induction reaction proceeded. In the early stage, both the aromatic and olefin products act as active HCP species and pentaMB was identified as the main aromatic HCP species. While in the latter stage of the induction period, the activity of olefins turned to much higher and pentaMB as well as hexaMB became the main aromatic HCP species. It was interestingly found that the reactivity of aromatics with larger molecular size like 1-E-pentaMB and hexaMB were much higher than that of lower methylbenzenes which indicates that the aromatic-based cycle can also proceed on the external acid site of HZSM-35 catalyst.

Acknowledgements

The authors thank the financial support from the National Natural Science Foundation of China (No. 21576256 and No. 21273005); Dr Linying Wang, Ms Yanli He and Ms Yanfei Zhang for sample characterization and beneficial discussion.

Notes and references

1 P. Tian, Y. X. Wei, M. Ye and Z. M. Liu, *ACS Catal.*, 2015, **5**, 1922–1938.
2 M. Stocker, *Microporous Mesoporous Mater.*, 1999, **29**, 3–48.
3 J. F. Haw, W. G. Song, D. M. Marcus and J. B. Nicholas, *Acc. Chem. Res.*, 2003, **36**, 317–326.
4 K. Y. Lee, H. K. Lee and S. K. Ihm, *Top. Catal.*, 2010, **53**, 247–253.
5 K. Hemelsoet, J. Van der Mynsbrugge, K. De Wispelaere, M. Waroquier and V. Van Speybroeck, *ChemPhysChem*, 2013, **14**, 1526–1545.
6 L. Qi, Y. X. Wei, L. Xu and Z. M. Liu, *ACS Catal.*, 2015, **5**, 3973–3982.
7 N. Tajima, T. Tsuneda, F. Toyama and K. Hirao, *J. Am. Chem. Soc.*, 1998, **120**, 8222–8229.

8 S. R. Blaszkowski and R. A. vanSanten, *J. Am. Chem. Soc.*, 1997, **119**, 5020–5027.
9 D. Lesthaeghe, V. Van Speybroeck, G. B. Marin and M. Waroquier, *Chem. Phys. Lett.*, 2006, **417**, 309–315.
10 D. Lesthaeghe, V. Van Speybroeck, G. B. Marin and M. Waroquier, *Angew. Chem., Int. Ed.*, 2006, **45**, 1714–1719.
11 S. Svelle, F. Joensen, J. Nerlov, U. Olsbye, K. P. Lillerud, S. Kolboe and M. Bjorgen, *J. Am. Chem. Soc.*, 2006, **128**, 14770–14771.
12 M. Bjorgen, S. Svelle, F. Joensen, J. Nerlov, S. Kolboe, F. Bonino, L. Palumbo, S. Bordiga and U. Olsbye, *J. Catal.*, 2007, **249**, 195–207.
13 I. M. Dahl and S. Kolboe, *J. Catal.*, 1994, **149**, 458–464.
14 I. M. Dahl and S. Kolboe, *J. Catal.*, 1996, **161**, 304–309.
15 I. M. Dahl and S. Kolboe, *Catal. Lett.*, 1993, **20**, 329–336.
16 W. G. Song and J. F. Haw, *Angew. Chem., Int. Ed.*, 2003, **42**, 892–894.
17 W. G. Song, J. F. Haw, J. B. Nicholas and C. S. Heneghan, *J. Am. Chem. Soc.*, 2000, **122**, 10726–10727.
18 U. Olsbye, S. Svelle, M. Bjorgen, P. Beato, T. V. W. Janssens, F. Joensen, S. Bordiga and K. P. Lillerud, *Angew. Chem., Int. Ed.*, 2012, **51**, 5810–5831.
19 S. Ilias and A. Bhan, *J. Catal.*, 2012, **290**, 186–192.
20 M. Westgard Erichsen, S. Svelle and U. Olsbye, *J. Catal.*, 2013, **298**, 94–101.
21 K. De Wispelaere, K. Hemelsoet, M. Waroquier and V. Van Speybroeck, *J. Catal.*, 2013, **305**, 76–80.
22 S. Ilias and A. Bhan, *J. Catal.*, 2014, **311**, 6–16.
23 T. Xu and J. F. Haw, *J. Am. Chem. Soc.*, 1994, **116**, 7753–7759.
24 T. Xu, D. H. Barich, P. W. Goguen, W. G. Song, Z. K. Wang, J. B. Nicholas and J. F. Haw, *J. Am. Chem. Soc.*, 1998, **120**, 4025–4026.
25 W. G. Song, J. B. Nicholas and J. F. Haw, *J. Phys. Chem. B*, 2001, **105**, 4317–4323.
26 W. G. Song, D. M. Marcus, H. Fu, J. O. Ehresmann and J. F. Haw, *J. Am. Chem. Soc.*, 2002, **124**, 3844–3845.
27 W. G. Song, J. B. Nicholas, A. Sassi and J. F. Haw, *Catal. Lett.*, 2002, **81**, 49–53.
28 J. Z. Li, Y. X. Wei, J. R. Chen, P. Tian, X. Su, S. T. Xu, Y. Qi, Q. Y. Wang, Y. Zhou, Y. L. He and Z. M. Liu, *J. Am. Chem. Soc.*, 2012, **134**, 836–839.
29 S. T. Xu, A. M. Zheng, Y. X. Wei, J. R. Chen, J. Z. Li, Y. Y. Chu, M. Z. Zhang, Q. Y. Wang, Y. Zhou, J. B. Wang, F. Deng and Z. M. Liu, *Angew. Chem., Int. Ed.*, 2013, **52**, 11564–11568.
30 T. Mole, G. Bett and D. Seddon, *J. Catal.*, 1983, **84**, 435–445.
31 R. F. Sullivan, R. P. Sieg, G. E. Langlois and C. J. Egan, *J. Am. Chem. Soc.*, 1961, **83**, 1156–1160.
32 B. Arstad, S. Kolboe and O. Swang, *J. Phys. Chem. A*, 2005, **109**, 8914–8922.
33 J. B. Wang, Y. X. Wei, J. Z. Li, S. T. Xu, W. N. Zhang, Y. L. He, J. R. Chen, M. Z. Zhang, A. M. Zheng, F. Deng, X. W. Guo and Z. M. Liu, *Catal. Sci. Technol.*, 2016, **6**, 89–97.
34 S. Teketel, U. Olsbye, K. P. Lillerud, P. Beato and S. Svelle, *Microporous Mesoporous Mater.*, 2010, **136**, 33–41.
35 J. Z. Li, Y. X. Wei, Y. Qi, P. Tian, B. Li, Y. L. He, F. X. Chang, X. D. Sun and Z. M. Liu, *Catal. Today*, 2011, **164**, 288–292.
36 F. F. Wei, Z. M. Cui, X. J. Meng, C. Y. Cao, F. S. Xiao and W. G. Song, *ACS Catal.*, 2014, **4**, 529–534.
37 L. Y. Wang, P. Tian, Y. Y. Yuan, M. Yang, D. Fan, H. Zhou, W. L. Zhu, S. T. Xu and Z. M. Liu, *Microporous Mesoporous Mater.*, 2014, **196**, 89–96.
38 E. Borodina, F. Meirer, I. Lezcano-Gonzalez, M. Mokhtar, A. M. Asiri, S. A. Al-Thabaiti, S. N. Basahel, J. Ruiz-Martinez and B. M. Weckhuysen, *ACS Catal.*, 2015, **5**, 992–1003.
39 J. Z. Li, Y. X. Wei, J. R. Chen, S. T. Xu, P. Tian, X. F. Yang, B. Li, J. B. Wang and Z. M. Liu, *ACS Catal.*, 2015, **5**, 661–665.
40 L. Qi, J. Z. Li, Y. X. Wei, L. Xu and Z. M. Liu, *Catal. Sci. Technol.*, 2016, **6**, 3737.
41 Y. X. Wei, J. Z. Li, C. Y. Yuan, S. T. Xu, Y. Zhou, J. R. Chen, Q. Y. Wang, Q. Zhang and Z. M. Liu, *Chem. Commun.*, 2012, **48**, 3082–3084.
42 C. Wang, J. Xu, G. D. Qi, Y. J. Gong, W. Y. Wang, P. Gao, Q. Wang, N. D. Feng, X. L. Liu and F. Deng, *J. Catal.*, 2015, **332**, 127–137.
43 J. F. Haw, J. B. Nicholas, W. G. Song, F. Deng, Z. K. Wang, T. Xu and C. S. Heneghan, *J. Am. Chem. Soc.*, 2000, **122**, 4763–4775.
44 P. W. Goguen, T. Xu, D. H. Barich, T. W. Skloss, W. G. Song, Z. K. Wang, J. B. Nicholas and J. F. Haw, *J. Am. Chem. Soc.*, 1998, **120**, 2650–2651.
45 W. Wang, Y. J. Jiang and M. Hunger, *Catal. Today*, 2006, **113**, 102–114.
46 C. Wang, Y. Y. Chu, A. M. Zheng, J. Xu, Q. Wang, P. Gao, G. D. Qi, Y. J. Gong and F. Deng, *Chem.–Eur. J.*, 2014, **20**, 12432–12443.

